Title	On the simultaneous deployment of two single-particle mass spectrometers at an urban background and a roadside site during SAPUSS
Authors	Dall'Osto, M.;Beddows, D.;McGillicuddy, Eoin;Esser-Gietl, Johanna K.;Harrison, Roy M.;Wenger, John C.
Publication date	2016-08-02
Original Citation	Dall'Osto, M., Beddows, D. C. S., McGillicuddy, E. J., Esser-Gietl, J. K., Harrison, R. M. and Wenger, J. C. (2016) 'On the simultaneous deployment of two single-particle mass spectrometers at an urban background and a roadside site during SAPUSS', Atmospheric Chemistry and Physics, 16, pp.9693-9710. doi: 10.5194/acp-16-9693-2016
Type of publication	Article (peer-reviewed)
Link to publisher's version	http://www.atmos-chem-phys.net/16/9693/2016/ - 10.5194/acp-16-9693-2016
Rights	© 2016, the Author(s). This work is distributed under the Creative Commons Attribution 3.0 License. - https://creativecommons.org/licenses/by/3.0/
Download date	2024-04-25 09:07:42
Item downloaded from	https://hdl.handle.net/10468/4139

Atmos. Chem. Phys., 16, 9693–9710, 2016
www.atmos-chem-phys.net/16/9693/2016/
doi:10.5194/acp-16-9693-2016

Atmospheric Chemistry and Physics Open Access EGU

On the simultaneous deployment of two single-particle mass spectrometers at an urban background and a roadside site during SAPUSS

Manuel Dall'Osto[1,2], David C. S. Beddows[3], Eoin J. McGillicuddy[4], Johanna K. Esser-Gietl[3,a], Roy M. Harrison[3,5], and John C. Wenger[4]

[1]Institut de Ciències del Mar, Consejo Superior de Investigaciones Científicas (CSIC), Pg Marítim de la Barceloneta 37–49, 08003 Barcelona, Spain
[2]Institute of Environmental Assessment and Water Research (IDAEA) Consejo Superior de Investigaciones Científicas (CSIC) C/Jordi Girona 18–26 08034 Barcelona, Spain
[3]National Centre for Atmospheric Science, Division of Environmental Health and Risk Management, School of Geography, Earth and Environmental Sciences, University of Birmingham, Edgbaston, Birmingham, B15 2TT, UK
[4]Department of Chemistry and Environmental Research Institute, University College Cork, Ireland
[5]Department of Environmental Sciences/Center of Excellence in Environmental Studies, King Abdulaziz University, Jeddah, 21589, Saudi Arabia
[a]now at: Deutscher Wetterdienst, Meteorological Observatory Hohenpeißenberg, Hohenpeißenberg, Germany

Correspondence to: Manuel Dall'Osto (dallosto@icm.csic.es)

Received: 7 December 2015 – Published in Atmos. Chem. Phys. Discuss.: 5 February 2016
Revised: 17 May 2016 – Accepted: 8 June 2016 – Published: 2 August 2016

Abstract. The aerosol time-of-flight mass spectrometer (ATOFMS) provides size-resolved information on the chemical composition of single particles with high time resolution. Within SAPUSS (Solving Aerosol Problems by Using Synergistic Strategies), continuous ATOFMS measurements of ambient particles were made simultaneously at two urban locations: urban background (UB) site and roadside (RS) site in the city of Barcelona (Spain) from 17 September to 18 October 2010. Two different instrumental configurations were used: ATOFMS (TSI 3800) with a converging nozzle inlet (high efficiency at about 800–2000 nm) at the UB site and ATOFMS (TSI 3800-100) with an aerodynamic lens inlet (high efficiency at about 300–700 nm) at the RS site. This is the first time, to our knowledge, that two ATOFMS instruments have been deployed in the same field study. The different instrument configurations had an impact on the observed particle types at the two sites. Nevertheless, 10 particle types were detected at both locations, including local and regional elemental carbon (22.7–58.9 % of total particles), fresh and aged sea salt (1.0–14.6 %), local and regional nitrate-containing aerosols (3–11.6 %), local lead-containing metallic particles (0.1–0.2 %), and transported Fe-nitrate particles (0.8–2.5 %). The ATOFMS at the UB also characterized four particle types: calcium-containing dust (0.9 %), Saharan dust (1.3 %), vanadium-containing particles (0.9 %), and vegetative debris (1.7 %). By contrast, the high statistical counts of fine particles detected at the RS allowed identification of eight particle types. Four of these contained organic nitrogen of primary and secondary origin, which highlights the complex nature of the sources and processes that contribute to this aerosol chemical component. Aminium salts were found related to coarse sulfate-rich particle types, suggesting heterogeneous reaction mechanisms for their formation. The other four particle types mainly containing organic carbon were found spiking at different types of the day, also showing a complex single-particle mixing state relationship between organic carbon and nitrate. This ATOFMS study clearly shows that the composition of atmospheric fine particles in Barcelona, and likely other Mediterranean urban areas, is complex, with a wide range of local and regional sources combining with chemical processing to produce at least 22 different particle types exhibiting different tempo-

ral behaviour. The advantage of using two ATOFMS instruments is also demonstrated, with the nozzle-skimmer configuration enabling detection of coarse dust particles and the aerodynamic lens configuration allowing better identification of particles rich in organic carbon and amines. Overall, we find that organic nitrogen is a considerable fraction of the single particles detected, especially at the traffic-dominated RS site. Further studies are needed, especially at high time resolution, to better understand the sources and properties of particulate organic nitrogen.

1 Introduction

A substantial number of studies have shown a relationship between measures of particulate air pollution and a variety of adverse health indicators (WHO, 2004). Formulation of cost-effective air pollution control policies depends upon a sound knowledge of source contributions to ambient concentrations. Only with such knowledge can realistic cost-benefit evaluations be conducted. The major sources of ambient particles in most urban areas are primary emissions from road traffic and other fuel combustion, secondary particles arising from condensation or chemical processing, and resuspension of soils and road dusts (AQEG, 2005; Harrison et al., 2012). Marine aerosol can also contribute in coastal locations and the interactions of anthropogenic trace gases with natural aerosol (i.e. dust, sea salt) can also have significant effects on aerosol composition (Abbatt et al., 2012).

Measurement of particle composition by online mass spectrometry has developed extensively over the last 2 decades and is currently the fastest growing area of atmospheric aerosol research (Laskin et al., 2012). The aerosol time-of-flight mass spectrometer (ATOFMS) has been used in many previous field studies to determine the chemical constituents of atmospheric aerosols (Pratt and Prather, 2012). It can identify both refractory and non-refractory species in single particles and can provide size-resolved information on particle sources and atmospheric processing at high time resolution (Prather and Pratt, 2012; Laskin et al., 2012). The ATOFMS has been used in a number of recent field studies in urban areas of Europe (Dall'Osto and Harrison, 2012; Healy et al., 2013) to identify and characterize particles from a diverse range of anthropogenic sources including traffic, solid fuel burning, industry, soil and road dust, marine aerosol, and secondary aerosol formation processes. However, it is worthy of mention that ATOFMS source apportionment capabilities are limited by the difficulties in quantification of its outputs (Reilly et al., 2000; Schoolcraft et al., 2001). Nevertheless, single-particle analysis is an important analytical tool that allows us to determine how the myriad chemical constituents are distributed between individual particles (mixing state; Pratt and Prather, 2012). The ATOFMS has often reported a number of particle types, which at times are difficult to associate with a specific aerosol source (Pastor et al., 2003; Dall'Osto and Harrison, 2006, 2012).

The objective of the present manuscript is to report a detailed analysis of the ATOFMS particle types detected during a field measurement campaign carried out in Barcelona, Spain, as part of the SAPUSS (Solving Aerosol Problems by Using Synergistic Strategies) project. The ATOFMS cannot provide quantitative aerosol mass loading concentrations, but its strength relies in the fact that it can monitor in real-time variations in the single-particle composition. In other words, small variations in the particle mixing state results in a single-particle mass spectra. As a result, a number of atmospheric processes and aerosol sources can be monitored in real time. In this paper we discuss not only information on the mass spectra but also diurnal trends persisting over 4 weeks. Further information on the intensive field campaign can be found in the overview paper by Dall'Osto et al. (2013a). Two different ATOFMS instruments were deployed during the 4-week measurement period – one at a roadside (RS) site and the other at an urban background (UB) site. This is the first time an ATOFMS has been deployed in Spain and, to the best of our knowledge, it is also the first time (worldwide) that two ATOFMS instruments have been deployed simultaneously in the same field campaign. The similarities and differences in particle types detected at both sites is described in detail and attributed to a range of local and regional sources as well as to different chemical and physical processes.

2 Methods

2.1 Location

The SAPUSS field measurement campaign involved a large variety of instrumentation deployed simultaneously at a number of monitoring sites in Barcelona (Spain), between 17 September and 18 October 2010 (local time, UTC + 2) (Dall'Osto et al., 2013a). ATOFMS measurements were made at the two main SAPUSS supersites.

RS site was situated in a car park next to a major road (Carrer Urgell). The road, which crosses the city from south-east to north-west, is a street canyon composed of a two-way cycling path and a one-way four lane vehicle road. Vehicle intensity for the month of measurements was about 17 000 vehicles per day.

UB site was situated in a small park at the north-western periphery of the city centre. A main road (Avenida Diagonal, 127 000 vehicles day^{-1}) is located about 500 m away from the site.

The two sites were about 2 km from each other (Dall'Osto et al., 2013a). While the UB site was open to wind from all directions, the wind flow and turbulence at the RS site were partially affected by the nearby street canyons and vehicular traffic. Previous reports from the SAPUSS campaign, based on measurements of organic and elemental compo-

nents of the aerosol, indicate that the particle composition and thus sources are similar at both sites (Dall'Osto et al., 2013b; Alier et al., 2013). Specifically, six organic aerosol (OA) components were identified at both sites: two of primary anthropogenic origin, three of secondary origin, and one whose source was not clearly defined (Alier et al., 2013). Elemental analysis provided by particle-induced X-ray emission (PIXE) enabled identification of nine different aerosol sources at both sites: three of regional origin, three types of dust aerosols, and three types of industrial aerosols (Dall'Osto et al., 2013b).

2.2 Instrumentation

The mass spectrometers were housed in air-conditioned trailers at both sites. Sampling was performed ca. 4 m above ground using a quarter-inch internal diameter stainless steel tube fitted with a $PM_{2.5}$ cyclone. The sample air was dried (through a Nafion dryer, Perma-Pure, length 100 cm, relative humidity $< 40\,\%$) before arriving at the instruments. The two ATOFMS instruments used in this study had different configurations. The instrument deployed at the RS site was an ATOFMS TSI model 3800-100, in which particles are sampled through an orifice and accelerated through an aerodynamic lens to the sizing region of the instrument (Su et al., 2004). By contrast, the instrument at the UB site was an ATOFMS TSI model 3800 that utilized a converging nozzle inlet (Gard et al., 1997). Both instruments provide the aerodynamic diameter of particles sizes between about 100 nm and 3 µm by calculating their time of flight between two orthogonally positioned continuous wave lasers ($\lambda = 532$ nm). However, the transmission efficiencies of the two instruments are quite different. While the aerodynamic lens affords a much higher transmission efficiency for particles with diameters less than about 1 µm, its performance for larger particles is not as good as the converging nozzle inlet. Following the sampling and sizing, particles are transferred to the mass spectrometry region where a pulsed laser ($\lambda = 266$ nm, about 1 mJ pulse^{-1}) desorbs and ionizes material within the particle in the centre of the ion source of a bipolar reflectron time-of-flight mass spectrometry. Thus, positive and negative ion mass spectra of a single particle are obtained. Overall, during the SAPUSS field study the ATOFMS was operating for 68 and 97 % of the time at the UB and at the RS site, respectively. It is also worth noting that an intercomparison of the two instruments was attempted at the same site, but this could not be completed due to complex logistical and technical factors.

The two different inlet configurations (aerodynamic lens and nozzle skimmer) strongly affect the size distributions of the detected particles and the overall aerosol population (Gard et al., 1997; Su et al., 2004). Hence, only a qualitative description of the detected particles is presented in this study. Furthermore, the ATOFMS mass spectrum is qualitative in that the intensities of the mass spectral peaks are not directly proportional to the component mass but are dependent on the particle matrix, the coupling between the laser and the particle, as well as the shot-to-shot variability of the laser (Dall'Osto and Harrison, 2012). Recent studies (Jeong et al., 2011) report excellent correlations for inorganic species (sulfate, nitrate, and ammonium) but weaker ones between total organic and elemental carbon (EC) detected with ATOFMS and other instruments (Jeong et al., 2011). However, the ATOFMS can provide quantitative information on particle number as a function of composition, providing a measure of all particle components, and can be used to assess mixing state.

The ATOFMS datasets were imported individually into YAADA (Yet Another ATOFMS Data Analyzer) and single-particle mass spectra were grouped with adaptive resonance theory neural network, ART-2a (Song et al., 1999). The parameters used for ART-2a in this study were learning rate 0.05, vigilance factor 0.85, and 20 iterations. Further details of the parameters can be found elsewhere (Dall'Osto and Harrison 2006; Rebotier and Prather 2007). An ART-2a area matrix (AM) of a particle cluster represents the average intensity for each m/z for all particles within a group. An ART-2a AM therefore reflects the typical mass spectra of the particles within a group.

2.3 Meteorological parameters and air mass back-trajectory analysis

The study area is affected by a convergence of air masses with different characteristics: the cold air coming down from medium and high latitudes and the warm air coming up from tropical and subtropical latitudes (Dall'Osto et al., 2013a). Five air mass meteorological regimes were classified during the SAPUSS field study, following the procedure described in Dall'Osto et al. (2013b): Atlantic (ATL), European-Mediterranean (EUR), North African east (NAF_E), North African west (NAF_W), and Regional (REG). Furthermore, meteorological variables (atmospheric pressure, wind speed, wind direction, solar radiation, temperature, and relative humidity) were also recorded at UB and RS SAPUSS monitoring sites during the whole field study. For further details, the reader is referred to the SAPUSS overview paper (Dall'Osto et al., 2013a).

3 Results

3.1 ATOFMS particle detection efficiency

Overall, 890 873 particle mass spectra were apportioned at the RS and 221 139 at the UB. This large difference in detected particle numbers is likely a result of the combined effects of the location and detection efficiencies of both instruments. As shown in Fig. 1, the number and size distribution of the particles detected by the two mass spectrometers is quite different and reflects their expected performance char-

Table 1. ATOFMS particle clusters identified from the SAPUSS campaign.

Monitoring RS site	Particle type	Particle number	%	Monitoring UB site	Particle type	Particle number	%
Local and regional EC	EC_Aged_L	277 151	31.1	Local and regional EC	EC_Aged_L	52 074	23.8
	EC_Aged_R	202 227	22.7		EC_Aged_R	76 678	35.1
Secondary inorganic	LRT-NIT	102 909	11.6	Secondary inorganic	LRT-NIT	9982	4.6
	Loc-NIT	37 790	4.2		Loc-NIT	15 931	7.3
	LRT-SUL	52 420	5.9		LRT-SUL	6635	3.0
Sea salt	NaCl-NIT	75 204	8.4	Sea salt	NaCl-NIT	8166	3.7
	NaCl	8926	1.0		NaCl	31,853	14.6
Industry	Fe	7201	0.8	Industry	Fe	5564	2.5
	Pb	577	0.1		Pb	382	0.2
Combustion	K-CN	21 515	2.4	Combustion	K-CN	2778	1.3
Monitoring RS site	Particle type	Particle number	%	Monitoring UB site	Particle type	Particle number	%
RS particles	Amine (POA 58)	6698	0.8	UB particles	Soil-Saharan	2842	1.3
	Amine (SOA 114)	3672	0.4		Soil-Ca	2482	0.9
	Amine (SOA 59)	2141	0.2		Oil-V	1875	0.9
	Amine (EST 84)	4888	0.5		Veg-KP	3897	1.7
	Org. (Lub Oil)	16 273	1.8				
	Org. (OC-CHO)	42 680	4.8				
	Org. (Aro-NIT)	15 306	1.7				
	Org. (OC-NIT)	13 295	1.5				
Total RS		890 873	100	Total UB		221 139	100

acteristics (Gard et al., 1997; Su et al., 2004). The instrument with the aerodynamic lens detected considerably more particles below 1 µm, while particles larger than ca. 1.9 µm were only detected with the converging nozzle inlet. By running ART-2a, more than 300 clusters were found initially in both UB and RS datasets. Many were merged when they presented similar temporal trends, size distributions, and mass spectra (Dall'Osto and Harrison, 2006). By merging similar clusters, the total number of particle types describing the whole dataset was reduced to 18 and 14 at the RS and UB sites, respectively. Despite the different inlet configurations and sampling locations, the majority of the particles detected at both sites could be described by 10 common ATOFMS particle types, listed in Table 1. A number of other particle types were found only at one of the monitoring sites (eight at the RS site and four at the UB site), likely due to the different urban environments as well as the different detection efficiency of the two instruments (Table 1).

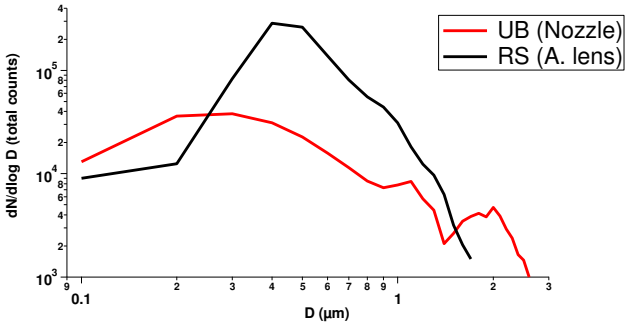

Figure 1. Size distributions of collected ATOFMS particles at the two SAPUSS monitoring sites.

3.2 ATOFMS particle types observed at both sites

3.2.1 Elemental carbon

Two main EC particle types, representing together more than 50 % of detected particles (58.9 % at the UB, 53.8 % at the RS), were identified at both sites. For reasons outlined below, they are named EC_Aged_R (regional) and EC_Aged_L (local). Both EC particle types presented a fine aerosol size distribution mode at both sites (about 300–500 nm; see Fig. S2 in the Supplement). Figure 2a shows the positive mass spectrum of particle type EC_Aged_R. It is dominated by EC peaks at m/z 12 $[C]^+$, 36 $[C_3]^+$, 48 $[C_4]^+$, and 60 $[C_5]^+$. Cluster EC_Aged_L (see Fig. 2b) also shows a similar EC positive mass spectrum pattern, although a strong signal at m/z 39 dominates the positive mass spectrum. This peak is often associated with potassium $[K]^+$, although there may also be a contribution from the organic ion $[C_3H_3]^+$ (Dall'Osto et al., 2009). The EC signals present in the positive mass spectra, and the near-total absence of peaks in the negative mass spectra suggests these EC particles are not

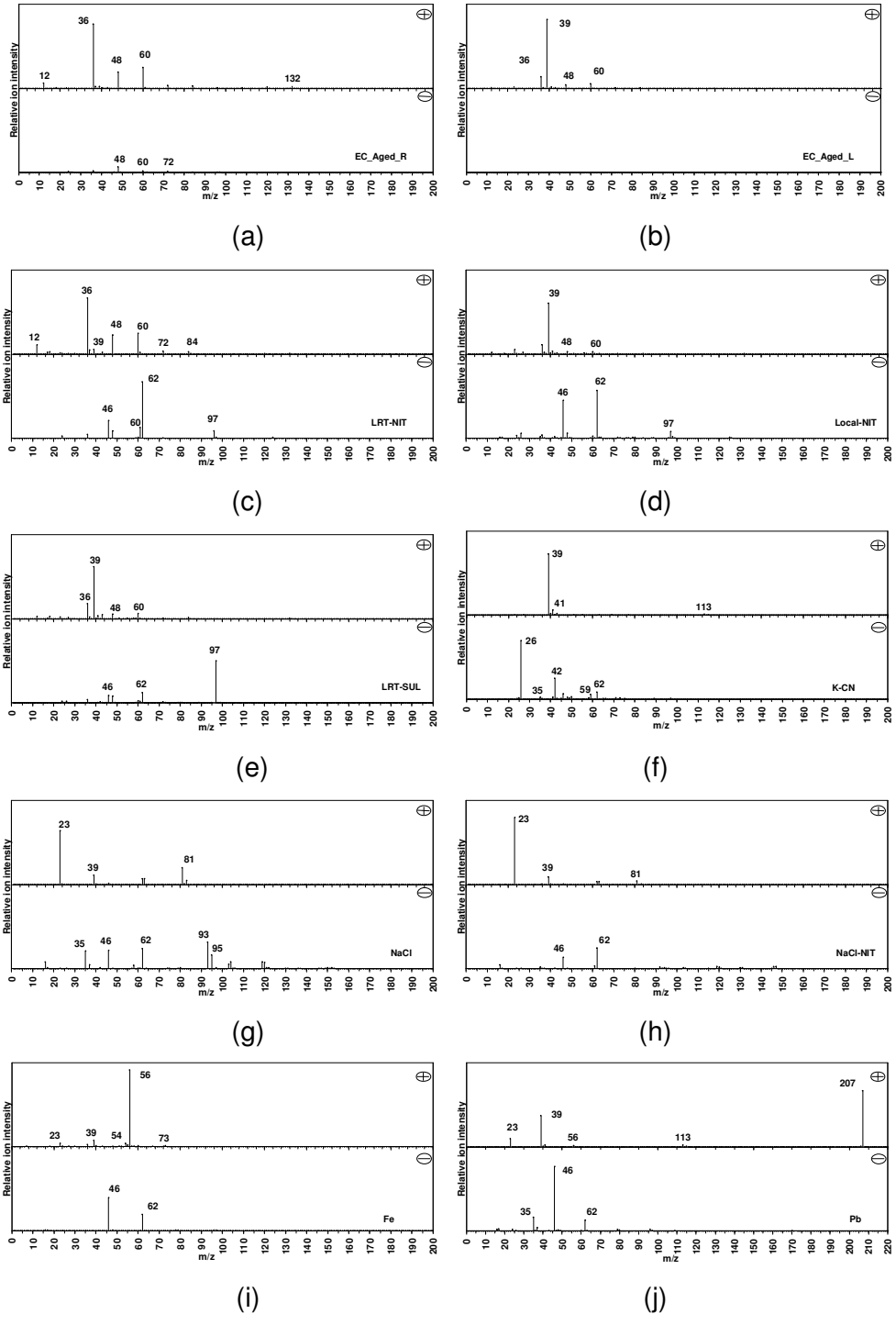

Figure 2. Average mass spectra of the 10 single-particle types observed at both the RS and UB sites.

freshly emitted. Indeed, Giorio et al. (2012) reported for a regional background site that strong EC peaks in the negative ion mass spectrum are more indicative of fresh emissions while strong EC peaks in the positive mode represent aged EC. This is consistent with observations which indicate that particle composition affects the ionization and fragmentation pattern of EC (Reinard and Johnson, 2008). The two EC-rich particle types were mainly detected in stagnant air masses. As shown in Fig. S1a, an enhancement of these particle types was observed during sulfate-rich air masses (7–10 October 2010) and nitrate-rich stagnant regional air masses (13–17 October 2010), as described in

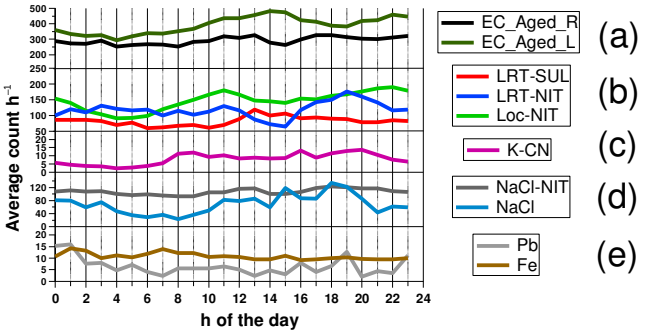

Figure 3. Diurnal profiles of the common particle types detected at both the RS and UB sites. Differences between RS and UB sites were minor and average diurnal profiles are presented.

Dall'Osto et al. (2013a). The diurnal profiles of these two aged EC particle types (Fig. 3a) can also help to classify their origin. Whilst EC_Aged_R shows little diurnal variation, particle type EC_Aged_L shows a gradual increase during the day, peaks in the afternoon (15:00 local time, LT), and drops to a minimum during night-time. The absence of sharp morning peaks indicates that these EC particle types are not associated with primary emission from local traffic. Similarly, the absence of a sharp evening peak also excludes the association with biomass burning, which is not expected at this time of the year and is generally not important in Barcelona (Dall'Osto et al., 2013a). Whilst the flat diurnal trend of EC_Aged_R is typical of regional aerosol, particle type EC_Aged_L suggests a local influence or an enhancement during the warmer part of the day. This assignment is also supported by the observed correlation of the EC types with some secondary inorganic particle types associated with local and regional aerosol sources, described in the next section. Similar conclusions were recently reported by Decesari et al. (2014), where most of the aged EC particles detected with the ATOFMS were related to aged anthropogenic aerosols accumulating in the lower layers of the Po Valley (Italy) overnight. Overall, we did not find major differences in the diurnal profiles of similar particle types detected simultaneously at the UB site and RS site. In other words, there were not major differences that could have been affected by wind speed and direction considering that the RS site is close to a large street canyon (Dall'Osto et al., 2013a).

3.2.2 Secondary nitrate and sulfate

The application of the ART-2a neural network algorithm to the ATOFMS data apportioned two main distinct nitrate particle types, already previously reported (Dall'Osto et al., 2009; Harrison et al., 2012; Decesari et al., 2014). The first (local nitrate (Loc-NIT); 4.2–7.3 % of particles by number) appears to be locally produced in urban locations during night-time, whilst the second (long-range transport – nitrate (LRT-NIT); 4.2–7.3 % of particles by number) is regionally transported within the Iberian Peninsula and the rest of Europe. Briefly, particle type Loc-NIT is characteristic of nitrate aerosol in small particles (D_a at about 300–500 nm; Fig. S2). The average mass spectrum (Fig. 2c) shows a peak at m/z 39 that can be due to potassium, although previous studies (Dall'Osto et al., 2009) suggested that an organic contribution may be also present depending on the m/z 39 / 41 ratio. The ATOFMS nitrate particle type appears to be associated with local formation processes and occurred in the main at times outside of the long-range transport episode (Fig. S2b). By contrast, a second nitrate particle type (LRT-NIT) is regionally transported. The average mass spectrum (Fig. 2d) shows that nitrate (m/z −62) is internally mixed with sulfate (m/z −97), ammonium (m/z 18) and both elemental (m/z 36, 48, 60) and organic carbon (m/z 37, 39, 43). As explained in Decesari et al. (2014) these aerosols likely originate from the night-time condensation of nitric acid on EC-containing primary particles (e.g. Shiraiwa et al., 2007). The LRT-NIT particle type is volatile, and partially evaporates during the day leaving a core of about 300 nm mainly composed also of sulfate, elemental and organic carbon (Dall'Osto et al., 2009). Indeed, this can be seen in the LRT-SUL (long-range transport – sulfate) particle type, whose average mass spectrum for this (Fig. 2e) shows peaks due to nitrate (m/z −62), sulfate (m/z −97), elemental carbon (m/z −36, 48, 60), and organic carbon (m/z −39, 43). The LRT-SUL and LRT-NIT diurnal trends are anticorrelated, as previously described elsewhere (Dall'Osto et al., 2009; Decesari et al., 2014), with LRT-SUL concentrations peaking in the afternoon hours. Such behaviour is attributed to the effect of the diel cycle of nitric acid and ammonia condensation/evaporation on the same particle type: during night-time this regional particle type is seen with nitrate, which evaporates during daytime, leaving a smaller aerosol core composed of EC and sulfate (Decesari et al., 2014). These two particle types were more abundant at the RS site, likely because of the improved focussing of smaller particles provided by the aerodynamic lens inlet. However, this study shows a novel aspect not found in the London local–regional nitrate study (Dall'Osto et al., 2009) or in the Po Valley (Decesari et al., 2014). During the period 12–14 October, under rainy conditions and with air masses arriving from Europe (Dall'Osto et al., 2013a), the transport of LRT-SUL was detected without the nitrate component (LRT-NIT, Fig. S1b). This could be due to a different source of LRT-SUL not linked with LRT-NIT and previously unobserved.

3.2.3 Potassium organonitrogen (K-CN) particles

The K-CN particle type was a minor one, representing only 1.3–2.4 % of the total particles analysed. Figure 2f shows the average mass spectrum, which features a strong peak at m/z 39 $[K]^+$ in the positive mode, as well as peaks at m/z 113 $[K_2Cl]^+$ and m/z −35 $[Cl]^-$, suggesting a biomass-burning source (Pastor et al., 2003; Dall'Osto and Harrison, 2006).

K-rich particles similar to K-CN have previously been attributed to biomass burning (Silva et al., 1999; Guazzotti et al., 2003) and were found to correlate with gas-phase measurements of acetonitrile, a good biomass-burning tracer. The negative ion mass spectrum shows strong peaks at m/z −26 $[CN]^-$ and m/z −42 $[CNO]^-$, indicating that the potassium and chloride are internally mixed with organonitrogen species. The size distribution, centred at about 350 nm (Fig. S2), also points to a combustion source. Overall, this particle type represented only about 2 % of the total particles sampled (Table 1) and its temporal variation is presented in Fig. S2d. Its diurnal trend (Fig. 3) tracks the anthropogenic activities of the city of Barcelona, suggesting general minor urban combustion processes. It should be noted that biogenic plant debris also has a similar single-particle mass spectrum, with strong signals at m/z 39, −26, and −42 (Silva and Prather, 2000). However, vegetative dust is usually internally mixed with sodium and phosphate and presents aerodynamic diameters above 1 µm (see Sect. 3.3).

3.2.4 Fresh and aged sea salt particles

Two sea salt particle types (fresh and aged) were detected at both sites, accounting for 9.4 and 18.3 % of the total particles sampled at RS and UB, respectively (Table 1). The higher percentage detected at the UB is likely due to the instrument configuration given that the nozzle inlet enables more efficient detection of coarser particles. The average mass spectrum (Fig. 2g) for the particle type assigned to fresh sea salt (labelled NaCl) shows peaks typical of sodium chloride clusters ($[Na]^+$ (m/z 23), $[K]^+$ (m/z 39), $[Na_2]^+$ (m/z 46), $[Na_2Cl]^+$ (m/z 81 and 83), $[NaCl_2]^-$ (m/z 93, 95 and 97)), whilst aged sea salt (NaCl-NIT, Fig. 2h) also exhibited nitrate peaks (m/z −46 and −62) reflecting the reaction between NaCl and HNO_3 and the replacement of chloride by nitrate (Gard et al., 1998). Both particle types had mean size distributions above 1 µm (Fig. S2c). NaCl was mainly detected during air masses that had travelled over Mediterranean regions (7–10 and 11–13 October), as shown in Fig. S2e. Interestingly, the diurnal variation of the two NaCl particle types is quite different (Fig. 3). Whilst NaCl-NIT does not show a clear trend, NaCl shows an enhancement in the afternoon, associated with the sea breeze, peaking at 15:00 (Dall'Osto et al., 2013c).

3.2.5 Iron- and lead-containing particles

Two common ATOFMS particle types have average mass spectra that were dominated by metals. The first was rich in iron (type Fe, 1.4 % of the total particles) and has a spectrum (Fig. 2i) characterized by a strong signal at m/z 56 and weaker features at m/z 73 (iron oxide, $[FeOH]^+$) and m/z 54 (isotope $[^{54}Fe]$). The negative spectrum has strong features at m/z −46 and −62, indicating that the iron is internally mixed with nitrate. During SAPUSS, the Fe particle type was found to correlate ($R^2 = 0.75$) with LRT-NIT, which is associated with long-range transport of pollutants. The small mode of the Fe particle type (Fig. S2) reflects the fact that only fine particles were likely to travel long distances relative to the coarser ones which were lost during transport. This is in line with previous ATOFMS field studies showing the transport of iron-containing particles internally mixed with nitrate from continental Europe (Harrison et al., 2012). The flat diurnal profile for the Fe particle type (Fig. 3) also suggests a regional origin. The long-range transport of fine Fe-containing particles (internally mixed with nitrate) is discussed further elsewhere (Dall'Osto et al., 2016).

The average mass spectrum of the second metal-rich particle type is shown in Fig. 2j. This particle type is labelled Pb since lead is one of the largest contributors in the positive mode, occurring at m/z +206, 207, and 208. Other peaks in the positive ion spectrum include m/z 23 $[Na]^+$, m/z 56 $[Fe]^+$, and m/z 39 and 113 ($[K]^+$ and $[K_2Cl]^+$). In addition to nitrate (m/z −46 $[NO_2]$ and m/z −62 $[NO_3]^-$), chloride (m/z −35 ($[Cl]^-$) was one of the most abundant species in the negative ion mode. Further information can be found in Dall'Osto et al. (2013b), where this ATOFMS particle type was found highly correlated with hourly elemental concentrations determined by PIXE analysis (Dall'Osto et al., 2013b), showing that this source of lead and chloride (Pb–Cl) is a major (82 %) source of fine Cl in the urban agglomerate of Barcelona. A similar particle type containing Pb–Cl was detected by ATOFMS in Mexico City and attributed to a waste incinerator source (Moffet et al., 2008), although other studies in the same area attributed lead-containing particles to multiple sources, including trash burning (Salcedo et al., 2010; Hodzic et al., 2012). It is worth noting that whilst the regional particle type Fe was mainly distributed in the fine mode (about 300–500 nm), a much larger mode (about 700–900 nm) was observed for this local ATOFMS Pb particle type (see Fig. S2d). Finally, the temporal trend (Fig. S1d) and the diurnal profile (Fig. 3) of the Pb particle type also suggests a local origin, likely related to emissions from urban combustion.

3.3 Particle types observed at UB

The ATOFMS fitted with converging nozzle inlet located at the UB site detected four particle types that were not observed at the RS site. Each of the particle types make a minor contribution (0.9–1.7 %) and overall they represented less than 5 % of the total particles sampled at the UB site.

3.3.1 Vanadium (V)-containing particles

A particle type containing vanadium (m/z 51 $[V]^+$ and m/z 67 $[VO]^+$) Na (m/z 23) and Fe (m/z 56), along with minor peaks due to EC at m/z 36, 48, and 60, was observed at the UB site. A negative ion mass spectrum was not acquired for this particle type (Fig. 4a). It has been shown that the

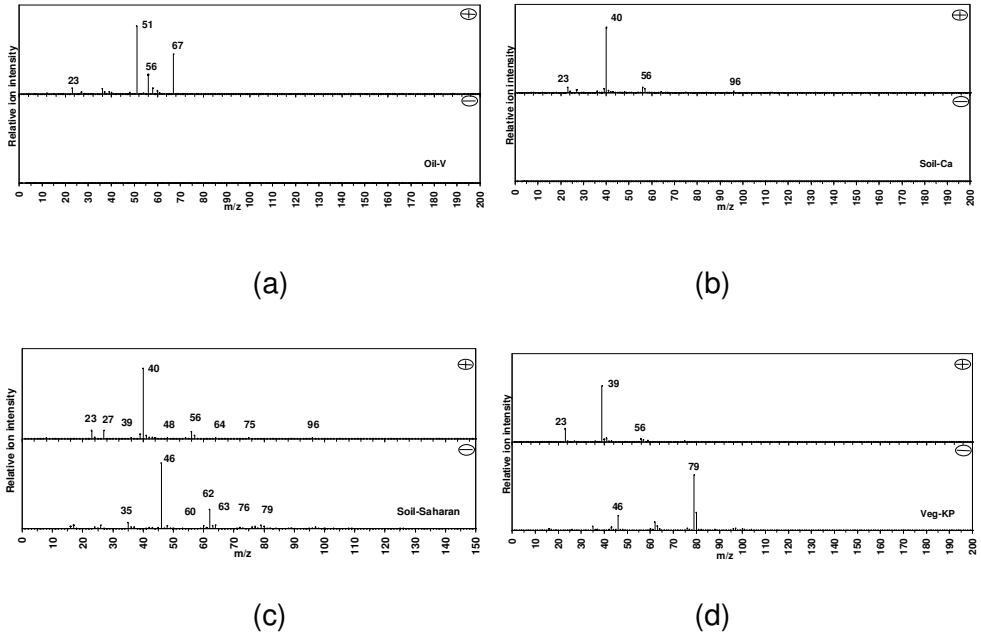

Figure 4. Average mass spectra of the four single-particle types only observed at the UB site.

condensation of secondary material on soot particles (Moffet and Prather, 2009) and the consequent change in aerosol hygroscopicity (Spencer et al., 2006) can suppress the formation of negative ions in real-time laser desorption/ionization mass spectrometry, causing many aged EC-containing particles to lack negative mass spectra (Neubauer et al., 1998). The V particle type accounted for only 1 % of the particles characterized at the UB, with a unimodal distribution peaking at about 350 nm pointing to a fresh combustion emission source. Field observations have confirmed that ships produce significant amounts of soot, vanadium, nickel, and sulfate (Pattanaik et al., 2007). Previous ATOFMS field measurements also reported that single particles containing organic carbon, vanadium, and sulfate (OC-V-sulfate) resulted from residual fuel combustion (i.e. bunker fuel), whereas high quantities of fresh soot particles represented distinct markers for plumes from distillate fuel combustion (i.e. diesel fuel) from ships as well as trucks in the port area (Healy et al., 2009; Ault et al., 2010). Indeed, the V particle type presented a temporal variation showing a maximum on 3 October 2010, when strong wind was blowing from the port of Barcelona (North African tropical air masses from the west (NAF_W); Fig. S1e). This Vanadium particle type is therefore most likely associated with fuel oil and ship emissions from the port. However, it was not detected at the RS site, possibly due to local street canyon effects which restrict transport and mixing in the area (Solazzo et al., 2008).

3.3.2 Soil rich in Ca (Soil-Ca)

The average ATOFMS mass spectrum of a dust particle type rich in calcium is shown in Fig. 4b, where peaks for calcium (m/z 40 $[Ca]^+$, 56 $[CaO]^+$, 57 $[CaOH]^+$, and 96 $[Ca_2O]^+$) are present. Peaks associated with sodium (m/z 23), magnesium (m/z 24, 25), and potassium (m/z 39) can also be seen. The Soil-Ca particle class represented 0.9 % of the particles sampled at the UB site and was found to moderately correlate ($R^2 = 0.6$) with the urban dust (Ca) factor obtained by PIXE-PMF analysis (Dall'Osto et al., 2013b). The large aerosol size mode above 1 µm (Fig. S1e) also points to a dust origin. Enhanced levels of the Ca ATOFMS particle type were observed during ATL air masses (Dall'Osto et al., 2013a), likely due to extra resuspension of dust caused by the high wind speeds during these periods. Urban areas in the south of Europe are known to have high dust loadings and three different types of dust were previously reported in the SAPUSS PIXE study (Dall'Osto et al., 2013b), representing ca. 25 % of the $PM_{2.5}$ mass concentrations measured. It should be noted that this particle type did not possess a negative ion mass spectrum and was also not detected at the RS site, likely for the same reasons explained above (Sect. 3.3.1).

3.3.3 Saharan dust particles (Saharan-dust)

A rarely observed particle type with peaks due to titanium at m/z 48 and 64 ($[Ti]^+$ and $[TiO]^+$, respectively) was found to represent 0.9 % of the particles sampled at the UB site (Fig. 4c). Additional peaks are associated with other metals including Na (m/z 23), Al (m/z 27), Ca (m/z 40, 56,

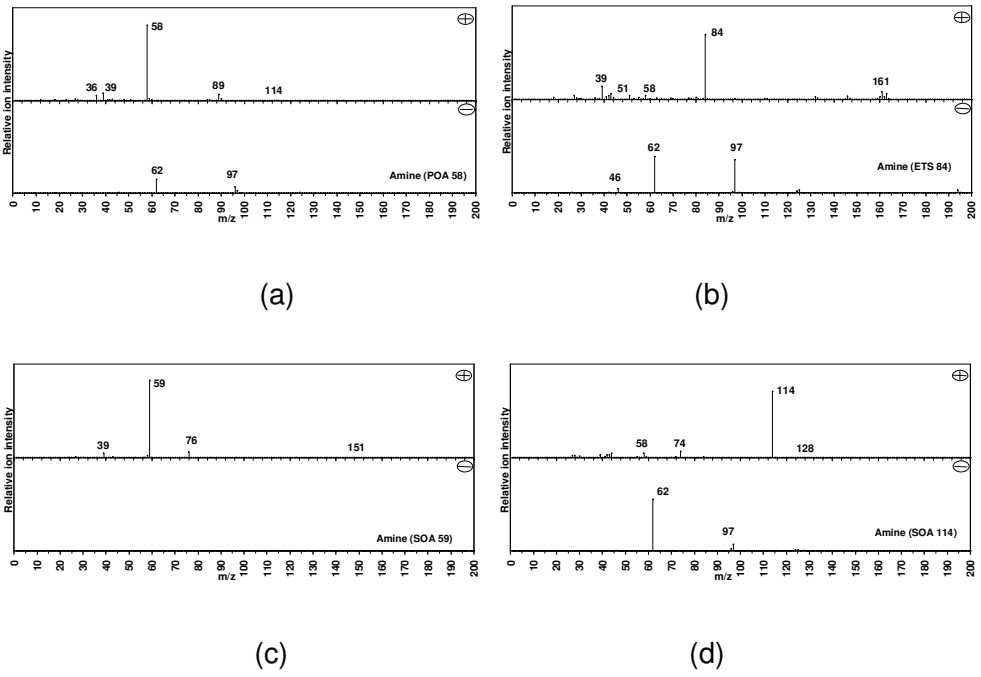

Figure 5. Average mass spectra of the four amine-containing single-particle types only observed at the RS site.

96), and Fe (m/z 56), as well as minor peaks of silicate at m/z −60 $[SiO_2]^-$ and −76 $[SiO_3]^-$. These particles presented an aerosol size coarse mode (1–3 µm; Fig. S2) and were detected mainly during the period 8–10 October, when Barcelona experienced air masses originating in the North African Saharan region (Dall'Osto et al., 2013a). It is likely that the Art-2a algorithm did not apportion this minor particle type of regional origin in the RS site. With regard to secondary species, it is interesting to note that the dust was internally mixed only with nitrate and not with sulfate (Fig. 4c). Previous studies (Dall'Osto et al., 2010) showed that Saharan dust particles collected near the Cape Verde Islands contained internally mixed nitrate but no sulfate, whilst Saharan dust particles collected on the coast of Ireland showed a very high degree of internally mixed secondary species including nitrate, sulfate, and methanesulfonate (Dall'Osto et al., 2004).

3.3.4 Vegetative debris (Veg-KP)

The ATOFMS has already proven to be a good tool for identifying and separating dust (mainly Ca-rich or Al-Si-rich) and biological particles (Fergenson et al., 2004). A particle type dominated by K (m/z 39) and phosphate (m/z −63 and −79) in the average mass spectrum (Fig. 4d) accounted for 1.7 % of the total particles sampled at the UB site. Strong signals at m/z 26 and 42, due to $[CN]^-$ and $[CNO]^-$, are also present, as well as peaks due to Na (m/z 23) and Fe (m/z 56). A coarse aerosol size mode of about 3 µm (Fig. S2) is likely again the reason why this particle type was not detected by the ATOFMS at the RS site. The size and chemical composition suggest a source such as vegetative debris and the particle type is thus labelled Veg K-P. A previous ATOFMS study reported a very similar particle type from samples of leaves collected from a roadside (Schofield, 2004). It is interesting to note that an increase of this vegetative debris particle type was detected under NAF_W air masses in concomitance with Saharan dust particles. Previous atmospheric measurements have shown that the concentration of bacteria over the sea may be much lower than over land but that higher concentrations of aerosolized microorganisms are generated during dust events compared to clean background marine conditions (Kellog and Griffin, 2006; Prospero et al., 2005).

3.4 Particle types observed at RS

The ATOFMS fitted with an aerodynamic focussing lens located at the RS site detected eight particle types that were not observed at the UB site.

3.4.1 Amines

Amines are ubiquitous in the atmospheric environment and have been detected in marine, urban, and rural atmosphere in the gas and particle phases as well as aqueous fog and rain water (Ge et al., 2011). The ATOFMS is a particularly good aerosol instrument for studying amines because the LDI laser wavelength (266 nm) ionizes them very efficiently (Angelino et al., 2001; Healy et al., 2015). During the SAPUSS measurement campaign, four amine particle types were detected at the RS. To the best of our knowledge, this is the first time

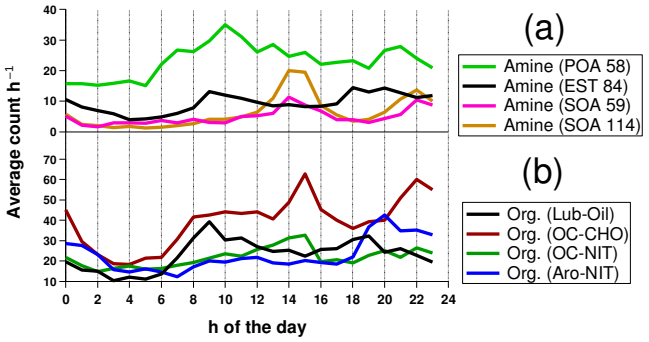

Figure 6. Diurnal trend of amines **(a)** and organic-rich **(b)** particle types detected at the RS site. Differences between RS and UB sites were minor and average diurnal profiles are presented.

such a variety of organonitrogen particle types has been detected at the single-particle level in real time in urban air.

a. *Amine (POA 58)*: Fig. 5a shows the ATOFMS mass spectra of a particle type called amine-58, which accounted for 0.8 % of the total particles classified at RS. The strongest peak in the positive mass spectra at m/z 58 is likely due to $[C_2H_5NH=CH_2]^+$. In general, the most important primary fragmentation process occurring for aliphatic amines involves the removal of one of the electrons from the lone pair on N and cleavage of the C–C bond to the nitrogen, with loss of the heavier alkyl group favoured. This cleavage explains the presence of the fragments at m/z 58 $[C_2H_5NH=CH_2]^+$, 72 $[C_3H_7NH=CH_2]^+$, 86 $[(C_2H_5)_2N=CH_2]^+$, and 114 $[(C_3H_7)_2N=CH_2]^+$. The minor peak at m/z 86 was found to correlate ($R^2=0.8$) with m/z 58. m/z 86 was suggested as amine species associated with fresh mobile emissions (Angelino et al., 2001). The negative mass spectrum shows nitrate and sulfate internally mixed with this particle type, although the former has a stronger signal than the latter. A size distribution peaking at about 300–400 nm was associated with this particle type. The diurnal variation of amine (POA 58) (Fig. 6a) shows a peak about 1 h later than morning and evening rush hour traffic and thus points to relatively fresh vehicular source. In conclusion, both the mass spectra (similar to previous traffic emissions; Angelino et al., 2001) and the temporal trend of this particle type point to traffic emission as a main source.

b. *Amine (ETS 84)*: Fig. 5b shows the average mass spectrum of a particle type associated with environment tobacco smoke (ETS) called amine-84, which represented 0.5 % of the total particles classified at RS. In the positive mass spectrum, the peak at m/z 161 is assigned to nicotine, with the main fragment being at m/z 84 (methyl-pyrrole fragment). The negative mass spectrum shows nitrate and sulfate internally mixed with this particle type. The amine-84 mass spectrum is very similar to that previously reported in Athens ($R^2=0.9$; Dall'Osto et al., 2007) and also attributed to tobacco smoke. This particle type generally followed human activity within the city (Fig. 6a), with a main peak in the morning (10:00) and a broader one during the evening (18:00–22:00 LT). It should be noted that an afternoon peak – potentially related to lunch activities – was not noticed. The ATOFMS cluster amine (ETS 84) attributed to tobacco smoke was compared to the measured nicotine value described in Alier et al. (2013). Briefly, much higher nicotine concentrations (58 ng m^{-3}) were observed at the RS site than at UB site (7 ng m^{-3}). This 8-fold difference pointed to a very high level of outdoor cigarette consumption near the RS site, which is situated next to a busy street and an exit of an underground metro station (Alier et al., 2013). Moreover, nicotine concentrations were more affected by daytime working activities during weekdays rather than during the weekends. ATOFMS cluster amine (ETS 84) was temporally correlated with nicotine concentrations available at 12 h resolution, and an R^2 of 0.65 was found, confirming the tobacco smoke source suggested. Spain ranks among the countries with the highest levels of cigarette consumption in the European Union and in the World (WHO, 2004; Alier et al., 2013). High outdoor gas-phase nicotine concentrations (0.5 and 1.5 µg m^{-3}) have been previously measured in Barcelona in summer 2010 (Sureda et al., 2012).

c. *Amine (SOA 59)*: Fig. 5c shows the average mass spectrum of a particle type called amine-59, which accounted for 0.2 % of the total particles classified at RS. Based on previous studies, the strong peak at m/z 59 ($[N(CH_3)_3]^+$) is attributed to trimethylamine (TMA) (Angelino et al., 2001; Healy et al., 2015). Amine (SOA 59) concentration was found particularly enhanced under regional air masses (13–17 October 2010, Fig. S1h) and exhibited a diurnal trend (Fig. 6a) showing maximum concentrations at 15:00 and 22:00. TMA plays an important role in atmospheric chemistry, yet its pathway towards aerosol is not clear. Rehbein et al. (2011) demonstrated that cloud/fog processing could enhance gas-to-particle partitioning of TMA. TMA can also participate in the formation of secondary organic aerosol. Several studies have shown that gas-phase TMA could form non-salt organic aerosol products through reaction with oxidizing agents (Murphy et al., 2007).

d. *Amine (SOA 114)*: Fig. 5d shows the average mass spectrum for a particle type called amine (SOA 114). The main peak is at m/z 114, which may be assigned to dipropylamine or tripropylamine (Angelino et al., 2001; Healy et al., 2015). Minor peaks can also be seen at m/z 58, 74, and 128, which were previously attributed

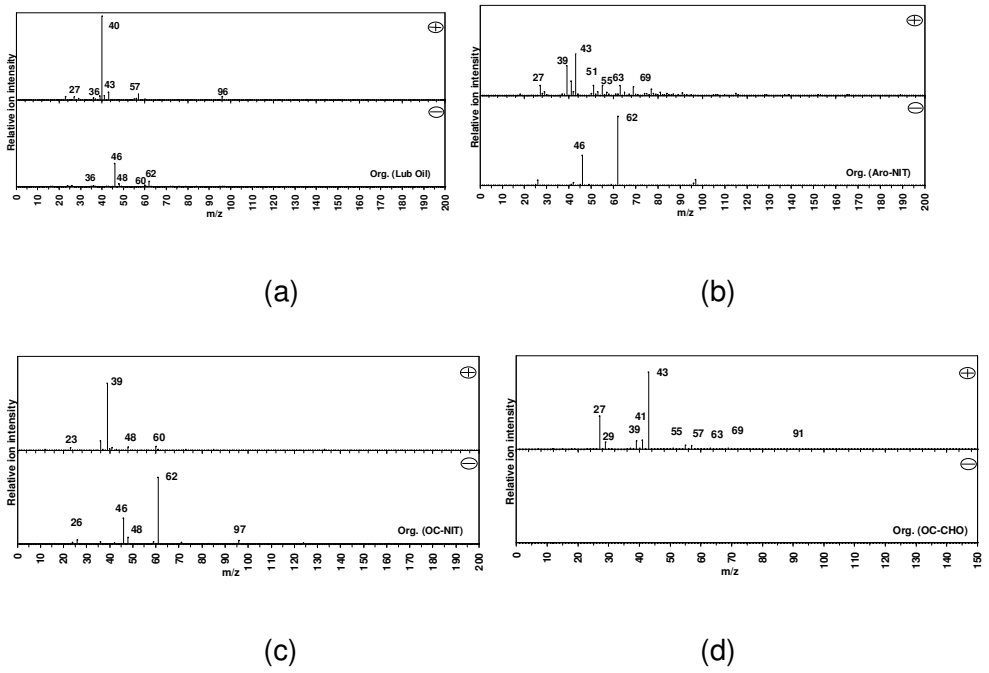

Figure 7. Average mass spectra of the four OC-rich single-particle types only observed at the RS site.

to alkyl ammonium nitrate salt particles formed by reaction of nitric acid and amines (Angelino et al., 2001). The negative ion mass spectrum for amine (SOA 114) shows a strong peak at m/z −62, confirming the presence of nitrate. Figure 6a shows that the diurnal profile is similar to that reported for amine (SOA 59), although with a much stronger peak at 15:00, during the warmest part of the day for the measurement period (Dall'Osto et al., 2013a). This is in line with recent measurements of gaseous amines by ambient pressure proton transfer reaction mass spectrometry (Hanson et al., 2011) which also showed an enhancement of TEA (triethylamine) during the afternoon. Amine (SOA 59) and amine (SOA 114) presented similar diurnal profiles but their temporal occurrence was not similar. Whilst amine (SOA 59) was detected mainly during the period of nitrate-rich regional air masses (13–17 October), amine (SOA 114) was detected mainly under NAF_E air masses rich in sulfate (7–10 October 2010). This observation is discussed further in Sect. 4.

Overall, the four amine-containing particle types were found distributed mainly in the sub-micron mode. Amine (POA 58) and amine (ETS 84), which are attributed to primary emissions from traffic and ETS respectively, have similar size distributions which peak around 400–500 nm (Fig. S2). Amine (SOA 59) and amine (SOA 114) were also found in the same size range, but presented a broader shape, suggesting partial condensation of SOA material on existing particles. Previous work of Angelino et al. (2001) used the peak at m/z 118 to track a marker for the oxidation products of alkylamines observed in the condensed phase of aerosol particles, specifically attributed to the oxidation of triethylamine (m/z 118; $[(C_2H_5)_2NCH_2]^+$). The analysis of the ATOFMS dataset for the RS site shows that the majority (about 80 %) of amine particle types containing a peak at m/z 118 were found in the tobacco-related ATOFMS amine (ETS 84) class, whereas the remaining 20 % was associated with amine (POA 58). This suggests – at least in our study – that m/z 118 cannot be used as a marker for amines produced by secondary processes. Other possible identification of higher mass ions detected and associated with organic nitrate include m/z 74 ($[C_2H_4NO_2]^+$), 88 ($[C_3H_6NO_2]^+$ or $([(C_2H_5)_2NO]^+$), 104 ($[C_3H_6NO_3]^+$), and 191($[C_6H_{11}N_2O_5]^+$). Overall, m/z 104 was found to be to be linked to amine (POA 58), whereas m/z 74 and 191 were related to amine (SOA 114). Finally, m/z 88 was found associated with both amine (POA 58) and amine (SOA 114). In summary, organic nitrate peaks were associated with both primary and secondary amine particle types.

3.4.2 Organic carbon (OC) particle types

The high efficiency of the ATOFMS equipped with the aerodynamic lens and deployed at the RS allowed us to characterize four particle types rich in organic compounds.

a. *Org (Lub. Oil)*: Fig. 7a shows the average mass spectrum of a particle type named "Lub. Oil" (1.8 %). The positive ion mass spectrum shows strong peaks for $[Ca]^+$ (m/z 40) and minor ones for OC (m/z 27, 43,

57) and EC (m/z 12, 24, 36, 48, 60). The negative mass spectrum shows the presence of nitrate (m/z −46, −62) and EC (−36, −48, −60). This particle type was only detected in the lower size range of the ATOFMS (ca. 150–400 nm), was found to spike during traffic rush hour times (Fig. 6b), and is attributed to lubricating oil from traffic emissions (Spencer et al., 2006; Drewnick et al., 2008).

b. Org. (*Aro-NIT)*: a particle type rich in aromatic compounds and internally mixed with nitrate (Org. (Aro-NIT)) was found to account for 1.7 % of the particles classified at the RS. The average mass spectrum shown in Fig. 7b features strong signals due to organic fragments at m/z 27, 29, 39, 43, 51, 57, and 63. m/z 51 $[C_4H_3]^+$, 63 $[C_5H_3]^+$, 77 $[C_6H_5]^+$, and 91 $[C_7H_7]^+$ are indicative of a strong aromatic signature (McLafferty, 1993). Common peaks due to nitrate (i.e. m/z −46 $[NO_2]^-$, m/z −62 $[NO_3]^-$) are found in the negative mass spectrum. Figure 6b shows a daily maximum of this particle type at about 19:00–20:00. Two previous ATOFMS studies in Athens (Dall'Osto and Harrison, 2006) and London (Dall'Osto and Harrison, 2012) reported very similar particle types (called C-SEC_2 and Na-EC-OC, respectively), which were attributed to condensation of organic compounds onto the particle phase as air temperatures dropped. The secondary particles showed clear internal mixing of organic and inorganic constituents. The size distribution of the Aro-NIT particle type shows a broad mode at about 500–700 nm (Fig. S2), also suggesting condensation of species on existing aerosols.

c. Org. (*OC-NIT)*: A third organic-rich particle type, called OC-NIT (1.5 % of the particles classified), was also detected at the RS site. Figure 7c shows the average positive ion mass spectrum, which contains a strong peak at m/z 39 (K and/or C_3H_3) and minor peaks due to OC and EC, as well as Na (m/z 23). Perhaps the most interesting part of the negative spectrum for this particle type is the presence of signals due to organic nitrogen species (m/z −26 $[CN]^-$ and m/z −42 $[CNO]^-$), not seen in other organic-rich particle types shown in Fig. 7. Finally, strong peaks for nitrate (m/z −46, −62) dominate the negative mass spectra. Figure 6b shows a daily maximum concentration of OC-NIT at 15:00. The presence of an organonitrogen component in this particle type, as well as its maximum at 15:00, is similar to that for the amine (SOA 59) particle type described in the previous section.

d. Org. (*OC-CHO)*: This particle type presents a positive mass spectrum (Fig. 7d), with strong peaks at m/z 27 $[C_2H_3]^+$ and m/z 43 $[(CH_3)CO]^+$ usually associated with oxidized secondary organic aerosol. Peaks at m/z 29 $[C_2H_5]^+$ and m/z 41 $[C_3H_5]^+$ confirm the strong hydrocarbon-like nature of the particles (Spencer et al., 2006), while weak peaks at m/z 51 $[C_4H_3]^+$, 63 $[C_5H_3]^+$, 77 $[C_6H_5]^+$, and 91 $[C_7H_7]^+$ also indicate an aromatic contribution (McLafferty, 1993). A negative ion mass spectrum was often not recorded for this particle type. However, some of the particles did generate one and an example is shown in Fig. S3d. The presence of peaks at m/z −45, −59, and −71 are likely to be due to the formate $[CHO_2]^-$, acetate $[C_2H_3O_2]^-$, and propionate $[C_3H_5O_2]^-$ ions, respectively. Figure 6b shows that in contrast to the other three OC-rich particle types, OC-CHO shows a complex diurnal profile. The number of counts per hour increases from 06:00 to 08:00 and then remains stable for about 5 h. A peak is observed around 15:00, the hottest part of the day, followed by a second peak at about 22:00–23:00. This diurnal profile is similar to that of amine (SOA 114), which is also of secondary origin. Cluster OC-CHO could also be associated with oxidation of aromatics by the OH radical (Platt et al., 2013; Giorio et al., 2015).

Overall these four OC-rich particle types indicate that a number of processes and sources are likely producing oxidized organic aerosols. There are at least four main peaks during the day: a morning traffic rush hour (09:00–10:00), an afternoon one during the hottest part of the day (15:00), and two evening ones at 20:00 (sunset) and at about 22:00–23:00. This is likely to be governed by a combination of emissions from local sources during rush hour periods, as well as by meteorological parameters such as atmospheric wind speed, wind direction, relative humidity, and temperature.

4 Discussion and conclusions

During the SAPUSS intensive field study two ATOFMS instruments were deployed simultaneously. The ATOFMS deployed at the RS site was equipped with an aerodynamic lens inlet system, allowing characterization of primary traffic aerosols as well as other primary and secondary aerosols affecting this heavily urbanized area of Barcelona. This type of ATOFMS (Su et al., 2004) has a very high efficiency in sampling aerosols (more than 1 000 000 single-particle mass spectra were collected at the RS), particularly for sub-micron particles in the size range 300–700 nm. The ATOFMS deployed at the UB site was equipped with a converging nozzle inlet system (Gard et al., 1997), which has a low aerosol collection efficiency (Dall'Osto et al., 2006), but it is particularly well suited for sampling coarser aerosols in the size range 800–2000 nm.

Overall, 10 particles types were detected at both sites (Table 1). Two of these particle types, composed of EC internally mixed with secondary inorganic species, described more than half of the classified single-particle mass spectra. EC_aged_R was found accumulating within stagnant air masses, with a flat diurnal profile and suggesting a certain

physico-chemical stability. In contrast, a more local but processed form of EC (EC_aged_L) was found to possess a finer submicron mode and enhanced concentrations during afternoon periods.

Two different types of nitrate-dominated aerosols were observed, in line with a previous ATOFMS study in London (Dall'Osto et al., 2009). The first (LRT_NIT) was attributed to regional nitrate (accumulation mode, volatile, more $NH_4NO_3/(NH_4)_2SO_4$ type) and the second (Loc_NIT) was assigned to local nitrate (ultrafine mode, less volatile, more OC-NO_3 type). An enhancement of local nitrate was found under warm and humid NAF_E air masses, indicating that meteorological conditions (i.e. high relative humidity) or aerosol composition (i.e. sea salt, Saharan dust) could affect local urban nitrate aerosol production.

Two types of sea salt particles were also identified at both sites. NaCl particles showed a peak in the diurnal profile at 15:00, related to the sea breeze and enhanced under NAF_E air masses. NaCl-NIT were mainly observed during more anthropogenically influenced air masses.

Two types of particles rich in metallic elements were found at both monitoring sites. One, rich in iron and internally mixed with nitrate, was found to be distributed in the fine accumulation mode at about 400 nm and related to regional air masses. This observation supports previous findings (Dall'Osto et al., 2010; Harrison et al., 2012) that showed fine iron-containing aerosols are able to travel long distances and are thus related to aged air masses. Other studies have reported anthropogenic Fe-containing particles internally mixed with secondary species such as sulfate (Furutani et al., 2011; Moffet et al., 2012) originating from coal combustion in Asian continental outflows. This study shows that – within the European continental outflow – Fe-containing particles are instead internally mixed with nitrate. This observed difference is likely due to emissions from coal combustion in Asia which are rich in SO_2, as opposed to European air masses which are relatively higher in NO_2 and lower in SO_2. Bio-available iron from atmospheric aerosol is an essential nutrient that can control ocean productivity (Baker and Croot, 2010). Hence, it can impact the global carbon budget and climate. There are also large uncertainties in the origin of the aerosol nitrogen matter which may be enhancing ocean productivity (Duce et al., 2008). The fact that iron is internally mixed with nitrate points to an urban source (i.e. more traffic than industrial activities) suggests that transported submicron urban particles can be a source of both iron and nitrogen nutrients for the oceans. However, it is worth noting that Cu-rich traffic-related aerosols can also have a negative effect on marine phytoplankton over a vast region of the western Mediterranean Sea (Jordi et al., 2012).

A second metallic particle type rich in lead and chloride was identified. This particle type was related to more local sources, presenting sharp spikes in concentration. It is interesting to note this particle type was found correlated with hourly elemental mass concentrations determined by PIXE analysis (Dall'Osto et al., 2013b), showing that this particle type can be a major source of submicron chloride in the urban area of Barcelona.

The ATOFMS equipped with the converging nozzle inlet at the UB site detected four further different particle types. Two types of dust particles were found, both occurring mainly in the coarse mode ($> 1\,\mu m$): one type, as attributed to Saharan Dust, was characterized by an aluminium/silicon signature, while the other type, with a more local origin (Ca dust), was characterized by a Ca-rich composition. Two other minor coarse particle types were characterized: Veg-KP (rich in potassium and phosphate), found enhanced during tropical NAF_E air masses, and vanadium-containing particles (Oil-V), related to shipping/oil combustion activities in the port of Barcelona. Overall, high concentrations of vanadium were only observed on 1 day (3 October), indicating that shipping emissions were a minor source of aerosol at the UB site.

Eight particle types were detected by the ATOFMS with aerodynamic focussing lens at the RS site. Overall, these particle types described less than 10 % of the aerosol population, but their mass spectra, as well as their peculiar diurnal profiles, allow us to advance our understanding of the OC-ON-nitrate mixing state of urban aerosols.

Four particle types contain amines, which, in addition to ammonia, are important atmospheric bases (Ge et al., 2011). Urban concentrations of ammonia in Barcelona are higher than those reported in similar urban background sites in Europe, especially in summer (Reche et al., 2012). Conversely, in winter, levels of ammonia were higher at traffic-affected sites, suggesting a contribution from vehicle emissions (Reche et al., 2012). Emissions of ammonia from vehicular traffic have been widely reported and they may increase in the future because it is not a regulated pollutant (Suarez-Bertoa et al., 2015). In comparison, the sources, atmospheric transformation, and sinks of amines are more poorly characterized. Overall, both primary (amine POA 58 and amine ETS 84) and secondary (amine SOA 59 and amine SOA 114) sources of amine-containing particles were identified during SAPUSS. The most abundant amine particle type (amine POA 58, 0.8 % of total particles at RS) was attributed to traffic activities and the second-most abundant (amine ETS 84, 0.5 % of the total particles at RS) was also associated with environmental tobacco smoke. Concurrent SAPUSS measurements (Alier et al., 2013) of nicotine concentrations were much higher at the RS site ($58\,ng\,m^{-3}$) than at UB ($7\,ng\,m^{-3}$), pointing to a significant outdoor cigarette consumption in the city centre. A recent study (Sleiman et al., 2010) found that nicotine can contribute significantly to the formation of urban SOA though reaction with ozone. The results of this study therefore suggest that third-hand cigarette smoke may be a source of nitrogen-containing particles in Barcelona and similar cities in southern Europe where smoking is prominent.

Amines were also related to secondary aerosol production, although a very complex dynamic was found associ-

ated with their occurrences. They were found to peak during the warmest part of the day (15:00) and during evening times (22:00–23:00). Amine (SOA 59) was found particularly enhanced in regional air masses (13–17 October 2010) when nitrate concentrations were also high (Dall'Osto et al., 2013b). By contrast, amine (SOA114) was more abundant in NAF_E humid air masses (7–11 October 2010). This latter type of SOA was internally mixed with nitrate, suggesting aminium salt formation under such specific conditions. Previous ATOFMS studies reported that most of the amines volatilized during cold seasons, whereas during summer most were in the form of low-volatility aminium nitrate and sulfate salts when particle acidity was higher (Pratt et al., 2009). This observation supports previous laboratory studies which reported that aerosol-containing non-salt organic amines are more stable and less volatile than nitrate salts (Murphy et al., 2007). Overall, amines can undergo oxidation by OH, O_3, and/or NO_3 to form amides, nitramines, and imines, which can also partition to the particle phase (Murphy et al., 2007; Silva et al., 2008; Healy et al., 2015). Rehbein et al. (2011) combined field and laboratory work to demonstrate that high relative humidity greatly enhances the gas-to-particle partitioning and subsequent aqueous acid–base reaction of amines. High relative humidity favours aqueous processing in general because aerosol is more likely to be in a deliquescent or partly deliquescent form (Saukko et al., 2015). During the SAPUSS study, we find aminium nitrate salts on coarse particles containing sulfate, suggesting that heterogeneous reactions occur during the warmest part of the day. This observation is in contrast to the study of Day et al. (2010), who reported organonitrates when sulfate aerosols and humidity were low, although the study site was less urbanized than the one used in this study.

Finally, some consideration should be given to the four specific organic particle types detected at the RS. One (Org. (Lub. Oil)) was found to be related to primary lubricating oil traffic emissions. More difficult is the attribution of the remaining three, which each contain an internal mixture of OC and nitrate. This is not surprising given the fact that the urban atmosphere is heavily contaminated by traffic emissions, the main producers of the two chemical species (Dall'Osto et al., 2013a).

Two different types of organic carbon/nitrate particle types were found. One (OC-NIT) was found spiking in the afternoon. By contrast, a nitrate with a strong aromatic signature (OC-Aro-NIT) was found mainly during night-time (80 % of the time) and showing a sharp concentration peak at 19:00–20:00. Part of the OC-Aro-NIT could be associated with products from the reaction of aromatic components with NO_3 radicals (Benton et al., 2010). These two ATOFMS particle types add complexity to the local–regional inorganic nitrate-containing particle types, and further studies are needed to correctly apportion the local urban nitrate component.

The fourth organic particle type (OC-CHO) was found rich in oxidized organic carbon and associated with nitrate from a traffic source. In a previous ATOFMS study, considerable effort was made to apportion cooking-related particle types (Dall'Osto and Harrison, 2012). However, only a particle type exhibiting maximum frequency during the warmest part of the day and associated with secondary aerosol production from traffic-related semi-volatile aromatic compounds was found. During this study, we were again not able to associate a specific particle type with cooking activities. In a companion SAPUSS study, Alier et al. (2013) reported an aerosol source formed mainly by C_7–C_9 dicarboxylic acids and detected especially during daytime, which is highly dynamic, dependent on air masses, and pointing to a secondary organic component driven by primary urban sources including cooking and traffic (mainly gasoline) activities. O'Brien et al. (2013) reported a detailed mass spectrometry characterization of the urban aerosol in an urban background environment. Compounds containing only carbon, hydrogen, and oxygen (CHO) and nitrogen-containing organic compounds (NOC) were found, showing that both photooxidation and ammonia chemistry may play a role in forming the compounds observed in the mixed urban–rural environment. NOC had precursor product pairs consistent with imidization and cyclization reactions, suggesting that part of the aromatic compounds detected during SAPUSS may also be formed by cyclization and not only by condensation of aromatic volatile organic compounds.

In summary, the two ATOFMS instruments deployed during the SAPUSS field measurement study showed that the urban atmosphere contains a complex mixture of aerosol particles emitted from a variety of sources and formed via numerous atmospheric processes. We have identified 22 different particle types, characterized by specific single-particle mass spectra and temporal trends. European Union abatement of traffic-related NO_x levels is still required to maintain levels within international standards (EEA, 2007). Higher NO_x levels (due to the high vehicle density and the high percentage of diesel vehicles) are often seen in urban background locations in Barcelona (and southern Europe) relative to other northern and central European cities (Eeftens et al., 2012). Latitude variations within Europe influence secondary nitrate aerosol formation (Revuelta et al., 2012). Organic nitrogen species represent a considerable fraction of fine particulate matter (Kiendler-Scharr et al., 2016). The present work shows a number of unique particle types detected mainly at the traffic-dominated RS site containing organic nitrogen and presenting different diurnal profiles, likely originating from different sources and different processes. Further studies are needed at high time resolution, emphasizing the need to better understand the sources and properties of particulate organic nitrogen. The ATOFMS measurements also provided some novel information on the mixing state of organic carbon and nitrate in urban aerosols, again highlighting the complex nature of the roles played by both primary sources and in situ chemical processing in affecting aerosol composition.

5 Data availability

Data are available by contacting the corresponding author.

The Supplement related to this article is available online at doi:10.5194/acp-16-9693-2016-supplement.

Acknowledgements. Financial support for this study was provided by the Marie Curie FP7 SAPUSS (FP7-PEOPLE-2009-IEF, Project number 254773) and previously supported by research projects from the D. G. de Calidad y Evaluacion Ambiental (Spanish Ministry of the Environment) and the Plan Nacional de IyD (Spanish Ministry of Science and Innovation) CGL2010-19464-VAMOS, CTQ2009-11572 and CTQ2009-377-14777-C02-01-AERTRANS). The SAPUSS team is also acknowledged.

Edited by: S. Decesari
Reviewed by: two anonymous referees

References

Abbatt, J. P. D., Leea, A. K. Y., and Thornton, J. A.: Quantifying trace gas uptake to tropospheric aerosol: recent advances and remaining challenges, Chem. Soc. Rev., 41, 6555–6581, 2012.

Alier, M., van Drooge, B. L., Dall'Osto, M., Querol, X., Grimalt, J. O., and Tauler, R.: Source apportionment of submicron organic aerosol at an urban background and a road site in Barcelona (Spain) during SAPUSS, Atmos. Chem. Phys., 13, 10353–10371, doi:10.5194/acp-13-10353-2013, 2013.

Angelino, S., Suess, D. T., and Prather, K. A.: Formation of aerosol particles from reactions of secondary and tertiary alkylamines: Characterization by aerosol time-of-flight mass spectrometry, Environ. Sci. Technol., 35, 3130–3138, 2001.

AQEG: Particulate matter in the UK, Defra, London, 2005.

Ault, A. P., Gaston, C. J., Wang, Y., Dominguez, G., Thiemens, M. H., and Prather, K. A.: Characterization of the Single Particle Mixing State of Individual Ship Plume Events Measured at the Port of Los Angeles, Environ. Sci. Technol., 44, 1954–1961, doi:10.1021/es902985h, 2010.

Baker, A. and Croot, P. L.: Atmospheric and marine controls on aerosol iron solubility in seawater, Mar. Chem., 120, 4–13, 2010.

Benton, A. K., Langridge, J. M., Ball, S. M., Bloss, W. J., Dall'Osto, M., Nemitz, E., Harrison, R. M., and Jones, R. L.: Night-time chemistry above London: measurements of NO_3 and N_2O_5 from the BT Tower, Atmos. Chem. Phys., 10, 9781–9795, doi:10.5194/acp-10-9781-2010, 2010.

Dall'Osto, M. and Harrison, R. M.: Chemical Characterisation of single airborne particles in Athens (Greece) by ATOFMS, Atmos. Environ., 40, 7614–7631, 2006.

Dall'Osto, M. and Harrison, R. M.: Urban organic aerosols measured by single particle mass spectrometry in the megacity of London, Atmos. Chem. Phys., 12, 4127–4142, doi:10.5194/acp-12-4127-2012, 2012.

Dall'Osto, M., Beddows, D. C. S., Kinnersley, R. P., Harrison, R. M., Donovan, R. J., and Heal M. R.: Characterization of individual airborne particles by using Aerosol Time-of-Flight Mass Spectrometry (ATOFMS) at Mace Head, Ireland, J. Geophys. Res., 109, D21302, doi:10.1029/2004JD004747, 2004.

Dall'Osto, M., Harrison, R. M., Beddows, D. C. S., Freney, E. J., Heal, M. R., and Donovan R. J.: Single-particle detection efficiencies of aerosol time-of-flight mass spectrometry during the North Atlantic marine boundary layer experiment, Environ. Sci. Technol., 40, 5029–5035, 2006.

Dall'Osto, M., Harrison, R. M., Charpantidou, E., Loupa, G., and Rapsomanikis, S.: Characterisation of indoor airborne particles by using real-time aerosol mass spectrometry, Sci. Total Environ., 384, 120–133, 2007.

Dall'Osto, M., Harrison, R. M., Coe, H., Williams, P. I., and Allan, J. D.: Real time chemical characterization of local and regional nitrate aerosols, Atmos. Chem. Phys., 9, 3709–3720, doi:10.5194/acp-9-3709-2009, 2009.

Dall'Osto, M., Harrison, R. M., Highwood, E. J., O'Dowd, C., Ceburnis, D., Querol, X., and Achterberg, E. P.: Variation of the mixing state of Saharan dust particles with atmospheric transport, Atmos. Environ., 44, 3135–3146, doi:10.1016/j.atmosenv.2010.05.030, 2010.

Dall'Osto, M., Querol, X., Alastuey, A., Minguillon, M. C., Alier, M., Amato, F., Brines, M., Cusack, M., Grimalt, J. O., Karanasiou, A., Moreno, T., Pandolfi, M., Pey, J., Reche, C., Ripoll, A., Tauler, R., Van Drooge, B. L., Viana, M., Harrison, R. M., Gietl, J., Beddows, D., Bloss, W., O'Dowd, C., Ceburnis, D., Martucci, G., Ng, N. L., Worsnop, D., Wenger, J., Mc Gillicuddy, E., Sodeau, J., Healy, R., Lucarelli, F., Nava, S., Jimenez, J. L., Gomez Moreno, F., Artinano, B., Prévôt, A. S. H., Pfaffenberger, L., Frey, S., Wilsenack, F., Casabona, D., Jiménez-Guerrero, P., Gross, D., and Cots, N.: Presenting SAPUSS: Solving Aerosol Problem by Using Synergistic Strategies in Barcelona, Spain, Atmos. Chem. Phys., 13, 8991–9019, doi:10.5194/acp-13-8991-2013, 2013a.

Dall'Osto, M., Querol, X., Amato, F., Karanasiou, A., Lucarelli, F., Nava, S., Calzolai, G., and Chiari, M.: Hourly elemental concentrations in $PM_{2.5}$ aerosols sampled simultaneously at urban background and road site during SAPUSS – diurnal variations and PMF receptor modelling, Atmos. Chem. Phys., 13, 4375–4392, doi:10.5194/acp-13-4375-2013, 2013b.

Dall'Osto, M., Ovadnevaite, J., Ceburnis, D., Martin, D., Healy, R. M., O'Connor, I. P., Kourtchev, I., Sodeau, J. R., Wenger, J. C., and O'Dowd, C.: Characterization of urban aerosol in Cork city (Ireland) using aerosol mass spectrometry, Atmos. Chem. Phys., 13, 4997–5015, doi:10.5194/acp-13-4997-2013, 2013c.

Dall'Osto, M., Beddows, D. C. S., Harrison, R. M., and Burcu, O.: Fine Iron Aerosols Are Internally Mixed with Nitrate in the Urban European Atmosphere, Environ. Sci. Technol., 50, 4212–4220, 2016.

Day, D. A., Liu, S., Russell, L. M., and Ziemann, P. J.: Organonitrate group concentrations in submicron particles with high nitrate and organic fractions in coastal southern California, Atmos. Environ., 44, 1970–1979, 2010.

Decesari, S., Allan, J., Plass-Duelmer, C., Williams, B. J., Paglione, M., Facchini, M. C., O'Dowd, C., Harrison, R. M., Gietl, J. K., Coe, H., Giulianelli, L., Gobbi, G. P., Lanconelli, C., Carbone, C., Worsnop, D., Lambe, A. T., Ahern, A. T., Moretti, F.,

Tagliavini, E., Elste, T., Gilge, S., Zhang, Y., and Dall'Osto, M.: Measurements of the aerosol chemical composition and mixing state in the Po Valley using multiple spectroscopic techniques, Atmos. Chem. Phys., 14, 12109–12132, doi:10.5194/acp-14-12109-2014, 2014.

Drewnick, F., Dall'Osto, M., and Harrison, R. M.: Characterization of aerosol particles from grass mowing by joint deployment of ToF-AMS and ATOFMS instruments, Atmos. Environ., 42, 3006–3017, 2008.

Duce, R. A., La Roche, J., Altieri, K., Arrigo, K. R., Baker, A. R., Capone, D. G., Cornell, S., Dentener, F., Galloway, J., Ganeshram, R. S., Geider, R. J., Jickells, T., Kuypers, M. M., Langlois, R., Liss, P. S., Liu, S. M., Middleburg, J. J., Moore, C. M., Nickovic, S., Oschlies, A., Pedersen, T., Prospero, J., Schlitzer, R., Seitzinger, S., Sorensen, L. L., Uematsu, M., Ulloa, O., Voss, M., Ward, B., and Zamora, L.: Impacts of atmospheric anthropogenic nitrogen on the open ocean, Science, 320, 893–897, 2008

EEA: EMEP/CORINAIR Atmospheric Emission Inventory Guidebook – 2007; European Environment Agency, available at: http://www.eea.europa.eu//publications/emep-eea-guidebook-2013 (last access: July 2016), 2007.

Eeftens, M., Tsai, M., Ampe, C., Anwander, B., Beelen, R., Bellander, T., Cesaroni, G., Cirach, M., Cyrys, J., de Hoogh, C., de Nazelle, A., de Vocht, F., Declercq, C., Dedele, A., Eriksen, K. T., Galassi, C., Grazuleviciene, R., Grivas, G., Heinrich, J., Hoffmann, B., Iakovides, M., Ineichen, A., Katsouyanni, K., Korek, M., Kramer, U., Kuhlbusch, T., Lanki, T., Madsen, C., Meliefste, K., Molter, A., Mosler, G., Nieuwenhuijsen, M., Oldenwening, M., Pennanen, A. S., Probst-Hensch, N., Quass, U., Raaschou, Nielsen O., Ranzi, A., Stephanou, E. G., Sugiri, D., Udvardy, O., Vaskovi, E., Weinmayr, G., Brunekreef, B., and Hoek, G.: Spatial variation of $PM_{2.5}$, PM_{10}, $PM_{2.5}$ absorbance and PMcoarse between and within 20 European study areas and the relationship with NO_2 – Results of the ESCAPE project, Atmos. Environ., 62, 303–317, 2012.

Fergenson, D. P., Pitesky, M. E., Tobias, H. J., Steele, P. T., Czerwieniec, G. A., Russell, D. H., Lebrilla, C. B., Horn, J. M., Coffee, K. R., Srivastava, A., Pillai, S. P., Shih, M.-T. P., Hall, H. L., Ramponi, A. J., Chang, J. T., Langlois, R. G., Estacio, P. L., Hadley, R. T., Frank, M., and Gard, E. E.: Reagentless Detection and Classification of Individual Bioaerosol Particles in Seconds, Anal. Chem., 76, 373–378, 2004.

Furutani, H., Jung, J., Miura, K., Takami, A., Kato, S., Kajii, Y., and Uematsu, M.: Single-particle chemical characterization and source apportionment of iron-containing atmospheric aerosols in Asian outflow, J. Geophys. Res., 116, D18204, doi:10.1029/2011JD015867, 2011.

Gard, E., Mayer, J. E., Morrical, B. D., Dienes, T., Fergenson, D. P., and Prather, K. A.: Real-time analysis of individual atmospheric aerosol particles: Design and performance of a portable ATOFMS, Anal. Chem., 69, 4083–4091, 1997.

Gard, E. E., Kleeman, M. J., Gross, D. S., Hughes, L. S., Allen, J. O., Morrical, B. D., Fergenson, D. P., Dienes, T., Galli, M. E., Johnson, R. J., Cass, G. R., and Prather, K. A.: Direct observation of heterogeneous chemistry in the atmosphere, Science, 279, 1184–1187, 1998.

Ge, X., Wexler, A. S., and Clegg, S. L.: Atmospheric amines – Part I. A review, Atmos. Environ., 45, 524–546, doi:10.1016/j.atmosenv.2010.10.012, 2011.

Giorio, C., Tapparo, M., Dall'Osto, M., Harrison, Roy, M., Beddows, D. C. S., Di Marco, C., Nemitz, E.: Comparison of three techniques for analysis of data from an Aerosol Time-of-Flight Mass Spectrometer, Atmos. Environ., 61, 316–326, 2012.

Giorio, C., Tapparo, A., Dall'Osto, M., Beddows, D. C., Esser-Gietl, J. K., Healy, R. M., and Harrison, R. M.: Local and regional components of aerosol in a heavily trafficked street canyon in central London derived from PMF and cluster analysis of single-particle ATOFMS spectra, Environ. Sci. Technol., 49, 3330–3340, 2015.

Guazzotti, S. A., Suess, D. T., Coffee, K. R., Quinn, P. K., Bates, T. S., Wisthaler, A., Hansel, A., Ball, W. P., Dickerson, R. R., Neususs, C., Crutzen, P. J., and Prather, K. A.: Characterization of carbonaceous aerosols outflow from India and Arabia: biomass/biofuel burning and fossil fuel combustion, J. Geophys. Res.-Atmos., 108, 4485, doi:10.1029/2002JD003277, 2003.

Hanson, D. R., McMurry, P. H., Jiang, J. K., Huey, G., and Tanner, D.: Ambient Pressure Proton Transfer mass spectrometry: detection of ammonia and amines, Environ. Sci. Technol., 45, 8881–8888, 2011.

Harrison, R. M., Dall'Osto, M., Beddows, D. C. S., Thorpe, A. J., Bloss, W. J., Allan, J. D., Coe, H., Dorsey, J. R., Gallagher, M., Martin, C., Whitehead, J., Williams, P. I., Jones, R. L., Langridge, J. M., Benton, A. K., Ball, S. M., Langford, B., Hewitt, C. N., Davison, B., Martin, D., Petersson, K. F., Henshaw, S. J., White, I. R., Shallcross, D. E., Barlow, J. F., Dunbar, T., Davies, F., Nemitz, E., Phillips, G. J., Helfter, C., Di Marco, C. F., and Smith, S.: Atmospheric chemistry and physics in the atmosphere of a developed megacity (London): an overview of the REPARTEE experiment and its conclusions, Atmos. Chem. Phys., 12, 3065–3114, doi:10.5194/acp-12-3065-2012, 2012.

Healy, R. M., O'Connor, I. P., Hellebust, S., Allanic, A., Sodeau, J. R., and Wenger, J. C.: Characterisation of single particles from in-port ship emissions, Atmos. Environ., 43, 6408–6414, 2009.

Healy, R. M., Sciare, J., Poulain, L., Crippa, M., Wiedensohler, A., Prévôt, A. S. H., Baltensperger, U., Sarda-Estève, R., McGuire, M. L., Jeong, C.-H., McGillicuddy, E., O'Connor, I. P., Sodeau, J. R., Evans, G. J., and Wenger, J. C.: Quantitative determination of carbonaceous particle mixing state in Paris using single-particle mass spectrometer and aerosol mass spectrometer measurements, Atmos. Chem. Phys., 13, 9479–9496, doi:10.5194/acp-13-9479-2013, 2013.

Healy, R. M., Evans, G. J., Murphy, M., Sierau, B., Arndt, J., McGillicuddy, E., O'Connor, I. P., Sodeau, J. R., and Wenger, J. C.: Single-particle speciation of alkylamines in ambient aerosol at five European sites, Anal Bioanal Chem., 407, 5899–5909, doi:10.1007/s00216-014-8092-1, 2015.

Hodzic, A., Wiedinmyer, C., Salcedo, D., and Jimenez, J. L.: Impact of trash burning on air quality in Mexico City, Environ. Sci. Technol., 46, 4950–4957, 2012.

Jeong, C.-H., McGuire, M. L., Godri, K. J., Slowik, J. G., Rehbein, P. J. G., and Evans, G. J.: Quantification of aerosol chemical composition using continuous single particle measurements, Atmos. Chem. Phys., 11, 7027–7044, doi:10.5194/acp-11-7027-2011, 2011.

Jordi, A., Basterretxea, G., Tovar-Sánchez, A., Alastuey, A., and Querol, X.: Copper aerosols inhibit phytoplankton growth in the

Mediterranean Sea, P. Natl. Acad. Sci. USA, 109, 21246–21249, doi:10.1073/pnas.1207567110, 2012.

Kellogg, C. A. and Griffin, D. W.: Aerobiology and the global transport of desert dust, Trends Ecol. Evol., 21, 638–644, doi:10.1016/j.tree.2006.07.004, 2006.

Kiendler-Scharr, A., Mensah, A. A., Friese, E., Topping, D., Nemitz, E., Prevot, A. S. H., Äijälä, M., Allan, J., Canonaco, F., Canagaratna, M., Carbone, S., Crippa, M., Dall Osto, M., Day, D. A., De Carlo, P., Di Marco, C. F., Elbern, H., Eriksson, A., Freney, E., Hao, L., Herrmann, H., Hildebrandt, L., Hillamo, R., Jimenez, J. L., Laaksonen, A., McFiggans, G., Mohr, C., O'Dowd, C., Otjes, R., Ovadnevaite, J., Pandis, S. N., Poulain, L., Schlag, P., Sellegri, K., Swietlicki, E., Tiitta, P., Vermeulen, A., Wahner, A., Worsnop, D., and Wu, H. C.: Organic nitrates from night-time chemistry are ubiquitous in the European submicron aerosol, Geophys. Res. Lett., doi:10.1002/2016GL069239, online first, 2016.

Laskin, A., Laskin, J., and Nizkorodov, S. A.: Mass spectrometric approaches for chemical characterization of atmospheric aerosols: critical review of the most recent advances, Environ. Chem., 9, 163–189, 2012

McLafferty, F. W.: Interpretation of Mass Spectra, 3rd Edn., p. 303, University Science Books, 1993.

Moffet, R. C. and Prather, K. A.: In-situ measurements of the mixing state and optical properties of soot with implications for radiative forcing estimates, P. Natl. Acad. Sci. USA, 106, 11872–11877, 2009.

Moffet, R. C., de Foy, B., Molina, L. T., Molina, M. J., and Prather, K. A.: Measurement of ambient aerosols in northern Mexico City by single particle mass spectrometry, Atmos. Chem. Phys., 8, 4499–4516, doi:10.5194/acp-8-4499-2008, 2008.

Moffet, R. C., Furutani, H., Rödel, T. C., Henn, T. R., Sprau, P. O., Laskin, A., Uematsu, M., and Gilles, M. K.: Iron speciation and mixing in single aerosol particles from the Asian continental outflow, J. Geophys. Res., 117, D07204, doi:10.1029/2011JD016746, 2012.

Murphy, S. M., Sorooshian, A., Kroll, J. H., Ng, N. L., Chhabra, P., Tong, C., Surratt, J. D., Knipping, E., Flagan, R. C., and Seinfeld, J. H.: Secondary aerosol formation from atmospheric reactions of aliphatic amines, Atmos. Chem. Phys., 7, 2313–2337, doi:10.5194/acp-7-2313-2007, 2007.

Neubauer, K. R., Johnston, M. V., and Wexler, A. S.: Humidity effects on the mass spectra of single aerosol particles, Atmos. Environ., 32, 2521–2529, 1998.

O'Brien, R. E., Laskin, A., Laskin, J., Liu, S., Weber, R., Russell, L., and Goldstein, A. H.: Molecular Characterization of Organic Aerosol Using Nanospray Desorption/Electrospray Ionization Mass Spectrometry: CalNex 2010 field study, Atmos. Environ., 68, 265–272, doi:10.1016/j.atmosenv.2012.11.056, 2013.

Pastor, S. H., Allen, J. O., Hughes, L. S., Bhave, P., Cass, G. R., and Prather, K. A.: Ambient single particle analysis in Riverside, California by aerosol time-of-flight mass spectrometry during the SCOS97-NARSTO, Atmos. Environ., 37, S239–S258, 2003.

Pattanaik, S., Huggins, F. E., Huffman, G. P., Linak, W. P., and Miller, C. A.: XAFS studies of nickel and sulfur speciation in residual oil fly-ash particulate matters (ROFA PM), Environ. Sci. Technol., 41, 1104–1110, 2007.

Platt, S. M., El Haddad, I., Zardini, A. A., Clairotte, M., Astorga, C., Wolf, R., Slowik, J. G., Temime-Roussel, B., Marchand, N., Ježek, I., Drinovec, L., Mocnik, G., Möhler, O., Richter, R., Barmet, P., Bianchi, F., Baltensperger, U., and Prévôt, A. S. H.: Secondary organic aerosol formation from gasoline vehicle emissions in a new mobile environmental reaction chamber, Atmos. Chem. Phys., 13, 9141–9158, doi:10.5194/acp-13-9141-2013, 2013.

Pratt, K. A. and Prather, K. A.: Mass spectrometry of atmospheric aerosols – Recent developments and applications, Part II: On-line mass spectrometry techniques, Mass Spectrom. Rev., 31, 17–48, 2012.

Pratt, K. A., Hatch, L. E., and Prather, K. A.: Seasonal volatility dependence of ambient particle phase amines, Environ. Sci. Technol., 43, 5276–5281, 2009.

Prospero, J., Blades, E., Mathison, G., and Naidu, R.: Interhemispheric transport of viable fungi and bacteria from Africa to the Caribbean with soil dust, Aerobiologia, 21, 1–19, 2005.

Rebotier, T. P. and Prather, K. A.: Aerosol time-of-flight mass spectrometry data analysis: A benchmark of clustering algorithms, Anal. Chim. Acta, 585, 38–54, 2007.

Reche, C., Viana, M., Pandolfi, M., Alastuey, A., Moreno, T., Amato, F., Ripoll, A., and Querol, X.: Urban NH_3 levels and sources in a Mediterranean environment, Atmos. Environ., 57, 153–164, 2012.

Rehbein, P. J. G., Jeong, C.-H., McGuire, M. L., Yao, X., Corbin, J. C., and Evans, G. J.: Cloud and fog processing enhanced gas-to-particle partitioning of trimethylamine, Environ. Sci. Technol., 45, 4346, doi:10.1021/ES1042113, 2011

Reilly, P. T. A., Lazar, A. C., Gieray, R. A., Whitten, W. B., and Ramsey, J. M.: The elucidation of charge-transfer-induced matrix effects in environmental aerosols via real-time aerosol mass spectral analysis of individual airborne particles, Aerosol Sci. Tech., 33, 135–152, 2000.

Reinard, M. S. and Johnston, M. V.: Ion formation mechanism in laser desorption ionization of individual particles, J. Am. Soc. Mass Spectr., 19, 389–399, 2008.

Revuelta, M. A., Harrison, R. M., Núñez, L., Gomez-Moreno, F. J., Pujadas, M., and Artíñano, B.: Comparison of temporal features of sulphate and nitrate at urban and rural sites in Spain and the UK, Atmos. Environ., 60, 383–391, 2012.

Salcedo, D., Onasch, T. B., Aiken, A. C., Williams, L. R., de Foy, B., Cubison, M. J., Worsnop, D. R., Molina, L. T., and Jimenez, J. L.: Determination of particulate lead using aerosol mass spectrometry: MILAGRO/MCMA-2006 observations, Atmos. Chem. Phys., 10, 5371–5389, doi:10.5194/acp-10-5371-2010, 2010.

Saukko, E., Zorn, S., Kuwata, M., Keskinen, J., and Virtanen, A.: Phase State and Deliquescence Hysteresis of Ammonium-Sulfate-Seeded Secondary Organic Aerosol, Aerosol Sci. Tech., 49, 531–537, 2015.

Schofield, M. J.: Sources and properties of airborne particulate matter, PhD Thesis, School of Geography, Earth and Environmental Sciences, Birmingham, University of Birmingham, 2004.

Schoolcraft, T. A., Constable, G. S., Jackson, B., Zhigilei, L. V., and Garrison, B. J.: Molecular dynamics simulations of laser disintegration of amorphous aerosol particles with spatially non-uniform absorption, Nucl. Instrum. Meth. B, 180, 245–250, 2001.

Silva, P. J. and Prather K. A.: Interpretation of mass spectra from organic compounds in aerosol time-of-flight mass spectrometry, Anal. Chem., 72, 3553–3562, 2000.

Silva, P. J., Liu, D.-Y., Noble, C. A., and Prather, K. A.: Size and chemical characterization of individual particles resulting from biomass burning of local Southern California species, Environ. Sci. Technol., 33, 3068–3076, 1999.

Silva, P. J., Erupe, M. E., Price, D., Elias, J., Malloy, Q. G. J., Li, Q., Warren, B., and Cocker, D. R.: Trimethylamine as precursor to secondary organic aerosol formation via nitrate radical reaction in the atmosphere, Environ. Sci. Technol, 42, 4689–4696, 2008.

Shiraiwa, M., Kondo, Y., Moteki, N., Takegawa, N., Miyazaki, Y., and Blake, D. R.: Evolution of mixing state of black carbonin polluted air from Tokyo, Geophys. Res. Lett., 34, L16803, doi:10.1029/2007GL029819, 2007.

Sleiman, M., Destaillats, H., Smith, J., Liu, C. L., Ahmed, M., Wilson, K. R., and Gundel, L. A.: Secondary organic aerosol formation from ozone-initiated reactions with nicotine and secondhand smoke, Atmos. Environ., 44, 4191–4198, 2010.

Solazzo, E., Cai, X., and Vardoulakis, S.: Modelling wind flow and vehicle-induced turbulence in urban streets, Atmos. Environ., 42, 4918–4931, 2008.

Song, X. H., Hopke, P. K., Fergenson, D. P., and Prather, K. A.: Classification of single particles analyzed by ATOFMS using an artificial neural network, ART-2A, Anal. Chem., 71, 860–865, 1999.

Spencer, M. T., Shields, L. G., Sodeman, D. A., Toner, S. M., and Prather, K. A.: Comparison of oil and fuel particle chemical signatures with particle emissions from heavy and light duty vehicles, Atmos. Environ., 40, 5224–5235, 2006.

Su, Y. X., Sipin, M. F., Furutani, H., and Prather, K. A.: Development and Characterization of an Aerosol Time-of-Flight Mass Spectrometer with Increased Detection Efficiency, Anal. Chem., 76, 712–719, 2004.

Suarez-Bertoa, R., Zardini, A. A., Lilova, V., Meyer, D., Nakatani, S., Hibel, F., Ewers, J., Clairotte, M., Hill, L., and Astorga, C.: Intercomparison of real-time tailpipe ammonia measurements from vehicles tested over the new world-harmonized light-duty vehicle test cycle (WLTC) Environ. Sci. Pollut. Res., 22, 7450–7460, 2015.

Sureda, X., Martinez-Sanchez, J. M., Lopez, M. J., Fu, M., Aguero, F., Salto, E., Nebot, M., and Fernandez, E.: Secondhand smoke levels in public building main entrances: outdoor and indoor $PM_{2.5}$ assessment, Tobacco Control, 21, 543–548, 2012.

WHO: Health Aspects of Air pollution, Syst. Rew. of health asp. of air poll. in Europe, WHO, Copenhagen, 2004.